Effects of normalized cross correlation on defect detection

D. M. Tsai and C. T. Lin
Machine Vision Lab.
Department of Industrial Engineering and Management
Yuan-Ze University, Chung-Li, Taiwan, R.O.C.
E-mail: iedmtsai@saturn.yzu.edu.tw

ABSTRACT

Normalized cross correlation (NCC) has been used extensively in machine vision for industrial inspection, but the traditional normalized correlation suffers from false alarms for the image that contains both complicated and uniform patterns in individual small regions. In this paper, we study the use of NCCs for defect detection in complicated images. The effect of NCCs in gray-level and color images, and the effect of image smoothing on the detection results are empirically evaluated. The proposed scheme can effectively alleviate false alarms in the implementation of NCC for defect detection.

Keywords: Normalized cross correlation; Defect detection; Color images; Smoothing

1. INTRODUCTION

Normalized cross correlation (NCC) has been a popular and easily implemented metric to evaluate the degree of similarity between two compared images. It is extensively used for many applications such as object recognition (Vijaya Kumar *et al.*, 2002; Tsi and Chiang, 2002), OCR (Lasko and Hauser, 2001; Wakahara *et al.*, 2001) and industrial inspections of printed circuit boards (Kim *et al.*, 1996), surface-mounted devices (Gallegos, *et al.*, 1996), wafers (Cai, *et al.*, 1994), printed-characters quality (Sato, *et al.*, 1991; Chang, *et al.*, 2001; Penz, *et al.*, 2001), fabrics (Yazdi and King, 1998), ceramic tiles (Costa and Petrou, 2000), and, aircraft engine x-ray data (Amladi *et al.*, 1991), etc.

In template matching application, the magnitude of the resulting NCC between two compared images are highly responsive to the changes in environmental conditions such as lighting and position of sensed objects. Ooi and Rao (1991) studied the effects of lighting, viewpoint and scale on the NCC for object recognition. They employed geometry and the physics of lighting and reflectance to examine the sensitivity of the NCC with change in position of the illumination source in gray level images. The behaviors of the NCC with changes in viewpoint and scale are analyzed for binary images. They showed that the analysis for gray-level images is mathematically intractable.

In this paper, we study the use of the NCC for defect detection in complicated images. The effect of the NCC in gray-level and color images, and the effect of image smoothing on the detection results are empirically evaluated. The proposed approach alleviates false alarms arising in the traditional NCC for defect detection. This paper is organized as follows: Section 2 presents the NCCs for both gray-level and color images. Section 3 first evaluates the effect the NCCs in gray-level and color images. The effect of image smoothing on NCC magnitude is then discussed. The paper is concluded in Section 4.

2. THE NCCs IN GRAY-LEVEL AND COLOR IMAGES

In the correlation-based defect detection application, a reference image and a scene image, both of sizes $M \times N$, are compared in a pixel-by-pixel basis. Two small windowed subimages of coincident pixel locations from the two respective images are used to compute the normalized cross correlation. The computation process is repeated by taking each coordinates (x, y) as the center of the neighborhood window so that the normalized correlation value of each pixel in the scene image can be evaluated. A pixel with NCC value below some specific threshold is then classified as a defective point. Local defects in the scene image can be segmented in this manner. False alarm or false acceptance may be generated if the NCC cannot provide distinct magnitudes to separate the regular and defective regions in the test image.

In gray-level images, the normalized cross correlation used for detecting defects between a reference image $t(i, j)$ and a scene image $f(x, y)$ is defined as

$$d_g(x,y) = \frac{\sum_{i=-m/2}^{m/2} \sum_{j=-n/2}^{n/2} f(x+i,y+j)\cdot t(x+i,y+j) - m\cdot n\cdot m_f \cdot m_t}{\left\{\left(\sum_i \sum_j f^2(x+i,y+j) - m\cdot n\cdot m_f{}^2\right)\cdot\left(\sum_i \sum_j t^2(x+i,y+j) - m\cdot n\cdot m_t{}^2\right)\right\}^{1/2}} \tag{1}$$

where $m\times n$ is the size of the neighborhood window; m_f and m_t are the gray-level averages of the windowed subimages from the scene and the reference, respectively, i.e.,

$$m_f = \frac{1}{m\cdot n}\sum_{i=-m/2}^{m/2}\sum_{j=-n/2}^{n/2} f(x+i,y+j)$$

$$m_t = \frac{1}{m\cdot n}\sum_{i=-m/2}^{m/2}\sum_{j=-n/2}^{n/2} t(x+i,y+j)$$

$d_g(x,y)$ gives the NCC of two compared subimages of size $m\times n$ at pixel coordinates (x, y). d_g for gray-level images is between –1 and 1, and the perfect match will have a maximum value of unity.

In manufacturing environment, defects on material surfaces are generally due to the abnormality of color and structure. Color provides powerful information for defect detection. The color of a pixel in the image is typically represented with the *RGB* values, corresponding to the red (*R*), green (*G*), and blue (*B*) frequency bands of the visible light spectrum. Let $R(x,y)$, $G(x,y)$ and $B(x,y)$ denote the *R*, *G* and *B* stimulus values, respectively, at pixel coordinates (x, y). Let

$$T(x,y) = \left(t_R(x,y), t_G(x,y), t_B(x,y)\right)$$

$$F(x,y) = \left(f_R(x,y), f_G(x,y), f_B(x,y)\right)$$

where $T(x,y)$ and $F(x,y)$ represent the *RGB* tristimulus vectors of the faultless reference pattern and the sensed subimages, respectively. The normalized cross correlation between the two color patterns $T(x,y)$ and $F(x,y)$ of size $m\times n$ is defined by

$$d_c(x,y)=\frac{s_{FT}(x,y)}{\{\,s_F(x,y)\cdot s_T(x,y)\,\}^{1/2}} \tag{2}$$

where

$$s_{FT}(x,y)=\sum_{i=-m/2}^{m/2}\ \sum_{j=-n/2}^{n/2}\ [\,F(x+i,y+j)\bullet T(x+i,y+j)\,]-3\cdot m\cdot n\cdot u_F\cdot u_T$$

$$s_F(x,y)=\sum_{i=-m/2}^{m/2}\ \sum_{j=-n/2}^{n/2}\ \|\,F(x+i,y+j)\,\|^2-3\cdot m\cdot n\cdot u_F^2$$

$$s_T(x,y)=\sum_{i=-m/2}^{m/2}\ \sum_{j=-n/2}^{n/2}\ \|\,T(x+i,y+j)\,\|^2-3\cdot m\cdot n\cdot u_T^2$$

and

$$u_F=\frac{1}{3\cdot m\cdot n}\sum_{i=-m/2}^{m/2}\ \sum_{j=-n/2}^{n/2}\ [\,f_R(x+i,y+j)+f_G(x+i,y+j)+f_B(x+i,y+j)\,]$$

$$u_T=\frac{1}{3\cdot m\cdot n}\sum_{i=-m/2}^{m/2}\ \sum_{j=-n/2}^{n/2}\ [\,t_R(x+i,y+j)+t_G(x+i,y+j)+t_B(x+i,y+j)\,]$$

$\langle\bullet\rangle$ and $\langle\|\cdot\|\rangle$ denote the inner product and the norm, respectively. The normalized cross correlation d_c for color images is also between –1 and 1.

3. THE EFFECT OF NCCs ON DEFECT DETECTION

3.1 The Effects of NCCs in Gray-Level and Color Images

The NCC d_g of eq. (1) uses only single gray-level information to evaluate the degree of similarity between two compared patterns in gray-level images. It is highly responsive to two compared patterns that contain only minor difference and, therefore, is well suited for detecting local small anomalies. However, the NCC d_g suffers from the false alarm when two compared patterns involve uniform images. For two uniform images, the variation of gray values in each image is relatively small. The association between two such images lacks of linear relationship, and may yield an NCC value approximate to zero accordingly.

Given a complicated image such as IC wafer and printed circuit board, some small region shows multiple gray-level (or color) patterns (e.g., a region with conductive paths) and the association between the reference and the sensed patterns will be linear. However, some small region in the test image appears to be uniform (e.g., a partial IC surface that contains no printed marks). The association between two uniform patterns could be nonlinear. The corresponding NCC value may be close to zero and result in false alarm in the inspection process.

Without loss of visibility, all test samples of both gray-level and color images are only displayed with gray-level images in this paper. The test images are 400×400 pixels, and the subimage window size used for NCC computation is 25×25 pixels. Figure 1 shows two IC images, of which Figure 1(a) is the reference image and Figure 1(b) is the scene image to be inspected. Figure 2(a) presents the resulting NCC value d_g for the gray-level version of the IC images as an intensity function (i.e., $d_g \cdot 255$ with 8-bit display). The brightness of each pixel in Figure 2(a) is proportional to the magnitude of d_g. Figure 2(b) displays the plot of the correlation function $(1-d_g) \cdot 255$ in 3D perspective. Figures 3(a) and 3(b) show the resulting NCC value d_c (eq.(2)) in 2D and 3D perspectives for the color version of the IC images. It can be seen from Figure 2 that all pixels around the central portion (containing printed characters) and those around the frame of the image (containing leads and conductive paths) involve complicated subimages and result in white regions (i.e., large correlation coefficients close to the unity) for both gray-level and color images. However, pixels in the uniform black surface of the IC generate darker regions (i.e., small correlation coefficients) in the resulting 2D plot for the gray-level version of the IC images. The 3D plot of the resulting d_g and d_c also reveal that d_g values from gray-level images are not reliable for measuring the similarity between two uniform patterns. d_c values from color images significantly improve the limitation of the d_g values from gray-level images.

In order to compare the quantitative difference between d_g and d_c, the signal-to-noise (SN) ratio is used in this study. It is defined as

$$SN_d = 20\left[\log_{10}\frac{S}{N}\right] \tag{3}$$

where S is the signal and N is the noise. Since the desired signal value (i.e., the correlation coefficient) is 1, the signal S is set to 1. The noise N is given by $1-u_d$, where u_d is the average of d_g or d_c of the entire sensed image. The larger the SN_d value, the better the improvement. Table 1 summarizes the d statistics and SN ratios from the gray-level and color images of the IC samples in Figure 1. It reveals that the average d_g value is 0.871 and the minimum d_g value is only 0.309 for gray-level images. This may result in false alarms in the inspection process, whereas the average d_c value is as high as 0.989 for color images. The SN ratio is significantly improved from 17.6 to 39.6 when color images are used for the computation of NCC.

3.2. The Effect of Smoothness

Although the correlation coefficients d_c derived from color images can significantly improve the interference of uniform patterns in defect detection, Figures 3(a) and 3(b) show that the resulting d_c is not a uniform white in the 2D plot of Figure 3(a), or not a flat horizontal plane in the 3D plot of Figure 3(b). In order to further improve the d_c measure and avoid false alarm in inspection, an image smoothing procedure on the original images is introduced in this study. The smoothing filter is a Gaussian one with varied filter sizes of 3×3, 5×5 and 7×7. The smoothing procedures are carried out for the original images of both the reference and the scene.

The IC samples in Figure 1 are used again to evaluate the effect of image smoothing on detection. Figures 4(a1)-(d1) and 4(a2)-(d2) present the resulting d_g in 2D and 3D perspectives for the gray-level images with the respective filter sizes of nil, 3×3, 5×5 and 7×7. Figures 4(a3)-(d3) show the histograms of d_g. The similar plots of the resulting d_c for color images are presented in Figure 5. Figure 4 demonstrates that the smoothing process cannot improve the effectiveness of d_g in gray-level images. The distributions of d_g in Figures 4(a3)-(d3) show that low d_g values still possess significant proportion, even though with the smoothing filter of size 7×7. The smoothing process for the color images has generated significant improvement. A uniform white intensity is obtained with the smoothing filter of size 5×5, as seen in Figure 5(c1). The distributions of d_c in color images also show that the improvement on high d_c values in Figures 5(a3)-(d3) is significant with only a small smoothing filter size of 3×3. Table 2 summarizes the resulting statistics and SN ratios of d_g and d_c for the test images in Figure 1. The SN ratios are not much improved for gray-level images, whereas the SN ratios are distinctly improved for the color images with smoothing.

One might suspect that the smoothing procedure may remove anomalies in the test image, and result in false acceptance. Figure 6 shows a defective version of the IC samples in Figure 1. The detection result of NCC d_c between the reference image in Figure 1(a) and the test image in Figure 6 in their color versions is demonstrated in Figure 7. It shows that the defect in the test image is well detected, either from the original image or the image with 7×7 smoothing. The noise is sufficiently removed from the images with increasing filter sizes.

Figure 8 shows an additional PCB sample for the test. Figure 8(a) is the reference image, and Figure 8(b) is the scene image that contains a subtle scratch of thin width. The detection results shown in 2D and 3D perspectives are presented in Figure 9. They reveal that the subtle defect is well distinctly enhanced, even with the smoothing filter of size 7×7.

4. CONCLUSION

In this paper, we have evaluated the use of NCCs for defect detection in both gray-level and color images. Experimental results show that the NCC from gray-level images may result in false alarms for two compared images with uniform patterns. The NCC derived from color images generates consistently high similarity values for two faultless images, compared to the one from gray-level images. This alleviates the false alarm that might encounter in gray-level images. A smoothing procedure on both reference and scene images can further improve the NCC consistence and reliability in color images. Experimental results also show that a small smoothing filter of size 3×3 is generally sufficient for the purpose. The normalized cross correlation from color images, along with the 3×3 smooth processing, provides an effective and easily-implemented referential approach for industrial inspection of defects in complicated images.

REFERENCES

Amladi, N. G., Finegan, M. K. Jr., Wee, W. G., 1991. Semiautomatic x-ray inspection system. In: Proceedings of SPIE, V. 1472, Orlando, FL, pp. 165-176.

Cai, X. Y., Kvasnik, F., Blore, R. W., 1994. Wafer fault measurement by coherent optical processor. Applied Optics 33, 4487-4496.

Chang, M.-C., Fuh, C.-S., Chen, H.-Y., 2001. Fast search algorithms for industrial inspection. International Journal of Pattern Recognition and Artificial Intelligence 15, 675-690.

Costa, C. E., Petrou, M., 2000. Automatic registration of ceramic tiles for the purpose of fault detection. Machine Vision and Applications 11, 225-230.

Gallegos, J. M., Villalobos, J. R., Carrillo, G., Cabrera, S. D., 1996. Reduced-dimension and wavelet processing of SMD images for real-time inspection. In: Proceedings of the IEEE Southwest Symposium on Image Analysis and Interpretation, San Antonio, TX, pp. 30-36.

Kim, J. H., Cho, H. S., Kim, S., 1996. Pattern classification of solder joint images using a correlation neural network. Engineering Applications of Artificial Intelligence 9, 655-669.

Lasko, T. A., Hauser, S. E., 2001. Approximate string matching algorithms for limited-vocabulary OCR output. In: Proceedings of SPIE, V. 4307, San Jose, CA, pp. 232-240.

Ooi, J., Rao, K., 1991. New insights into correlation-based template matching. In: Proceedings of SPIE, V. 1468, Applications of Artificial Intelligence IX, Orlando, FL, pp. 740-751.

Penz, H., Bajla, I., Vrabl, A., Krattenthaler, W, Mayer, K., 2001. Fast real-time recognition and quality inspection of printed characters via point-correlation. In: Proceedings of SPIE, V. 4303, San Jose, CA, pp. 127-137.

Sato, K., Kan'no, H., Ito, T., 1991. System for inspecting pad-printed characters using the normalized correlation of the segmented character images. In: Proceedings of the International Conference on Industrial Electronics, Control and Instrumentation-IECON' 91, Los Alamitos, CA, pp. 1929-1932.

Tsai, D.-M., Chiang, C.-H., 2002. Rotation-invariant pattern matching using wavelet decomposition. Pattern Recognition Letters 23, 191-201.

Vijaya Kumar, B. V. K., Venkataramani, K., Savvides, M., 2002. Efficient methods for correlation-based automatic target recognition. In: Proceedings of SPIE, V. 4726, Orlando, FL, pp. 183-192.

Wakahara, T., Kimura, Y., Tomono, A., 2001. Affine-invariant recognition of gray-scale characters using global affine transformation correlation. IEEE Transactions on Pattern Analysis and Machine Intelligence 23, 384-395.

Yazdi, H. R., King, T. G., 1998. Application of 'vision in the loop' for inspection of lace fabric. Real-Time Imaging 4, 317-332.

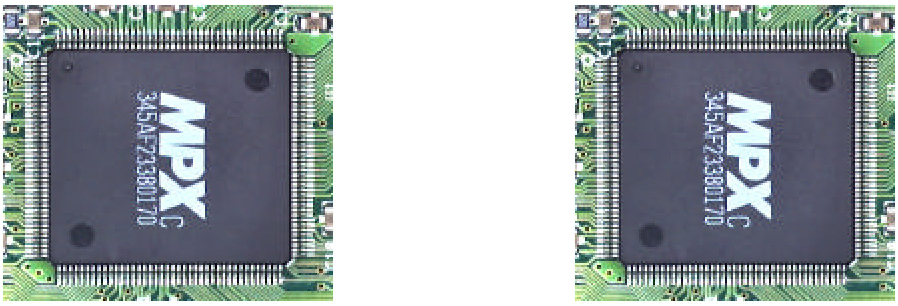

(a) (b)

Figure 1. An IC on the printed circuit board: (a) the reference image; (b) the scene image.

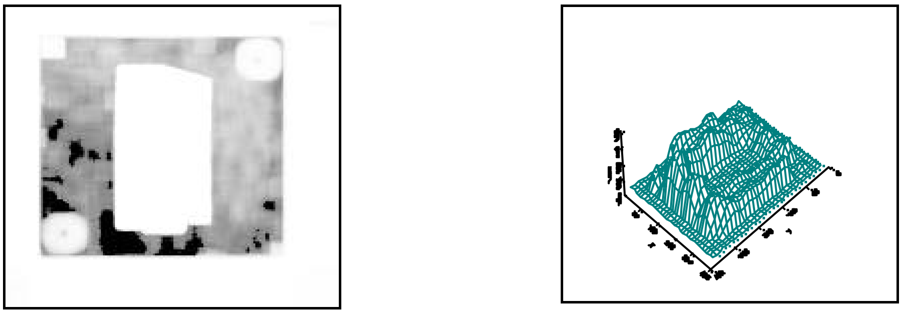

(a) (b)

Figure 2. The resulting NCC d_g from the gray-level version of the IC sample in Figure1: (a) the correlation values as an intensity function $d_g \times 255$; (b) the correlation function $(1-d_g)\times 255$ in 3-D perspective.

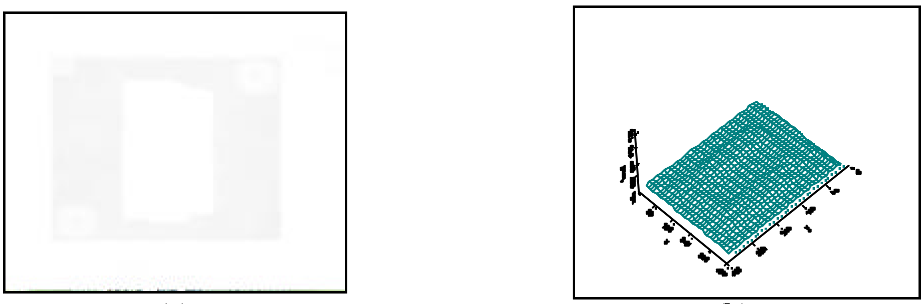

(a) (b)

Figure 3. The resulting NCC d_c from the color version of the IC sample in Figure1: (a) the correlation values as an intensity function $d_c \times 255$; (b) the correlation function $(1-d_c)\times 255$ in 3-D perspective.

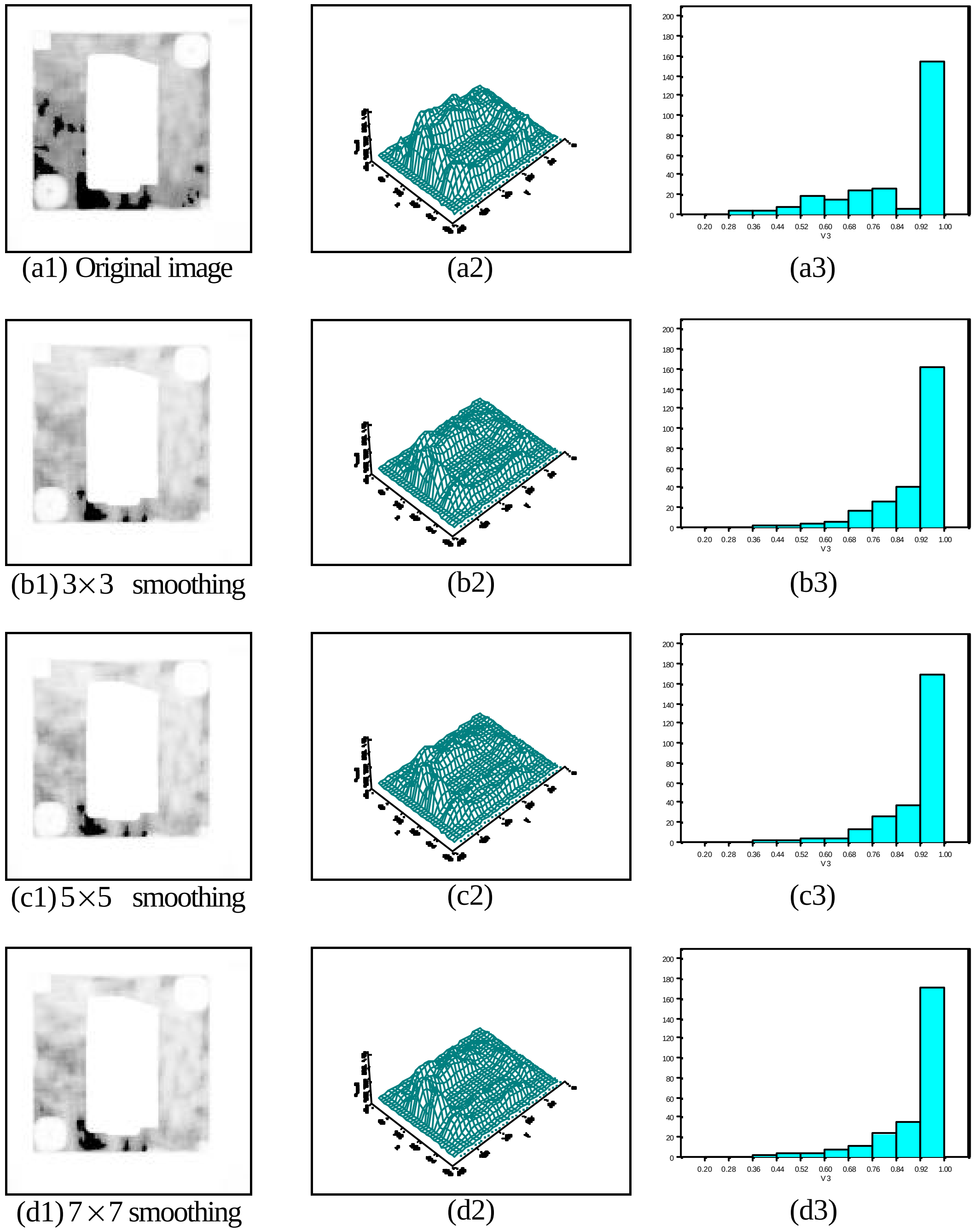

Figure 4. The effect of smoothing on faultless gray-level images in Figure1: (a1)-(d1) the correlation values as an intensity function with smoothing filter sizes of nil, 3×3, 5×5 and 7×7, respectively; (a2)-(d2) the respective correlation functions in 3-D perspective; (a3)-(d3) the respective histograms of d_g.

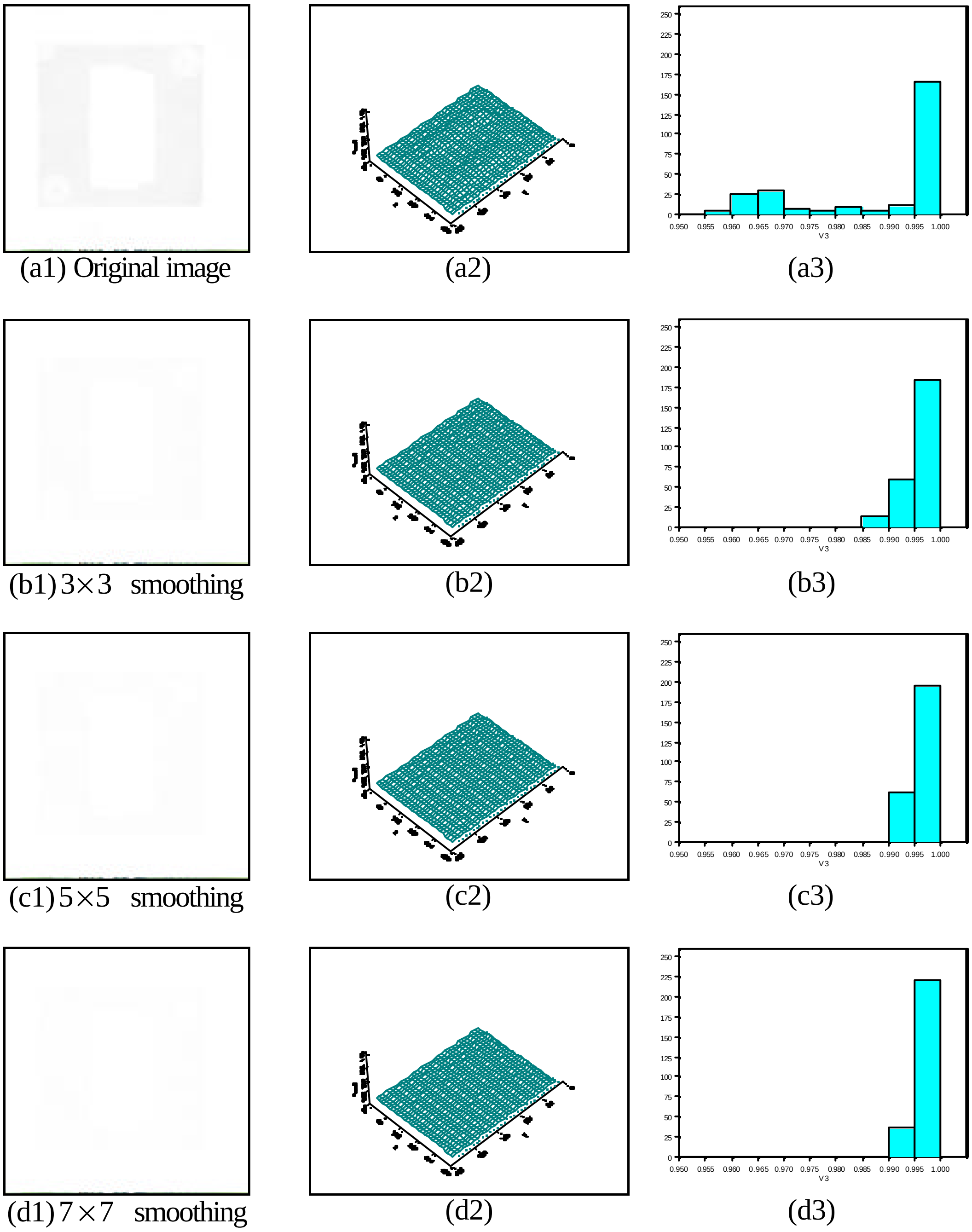

Figure 5. The effect of smoothing on faultless color images in Figure1: (a1)-(d1) the correlation values as an intensity function with smoothing filter sizes of nil, 3×3, 5×5, 7×7, respectively; (a2)-(d2) the respective correlation functions in 3-D perspective; (a3)-(d3) the respective histograms of d_c.

Figure 6. A defective version of the IC image in Figure1.

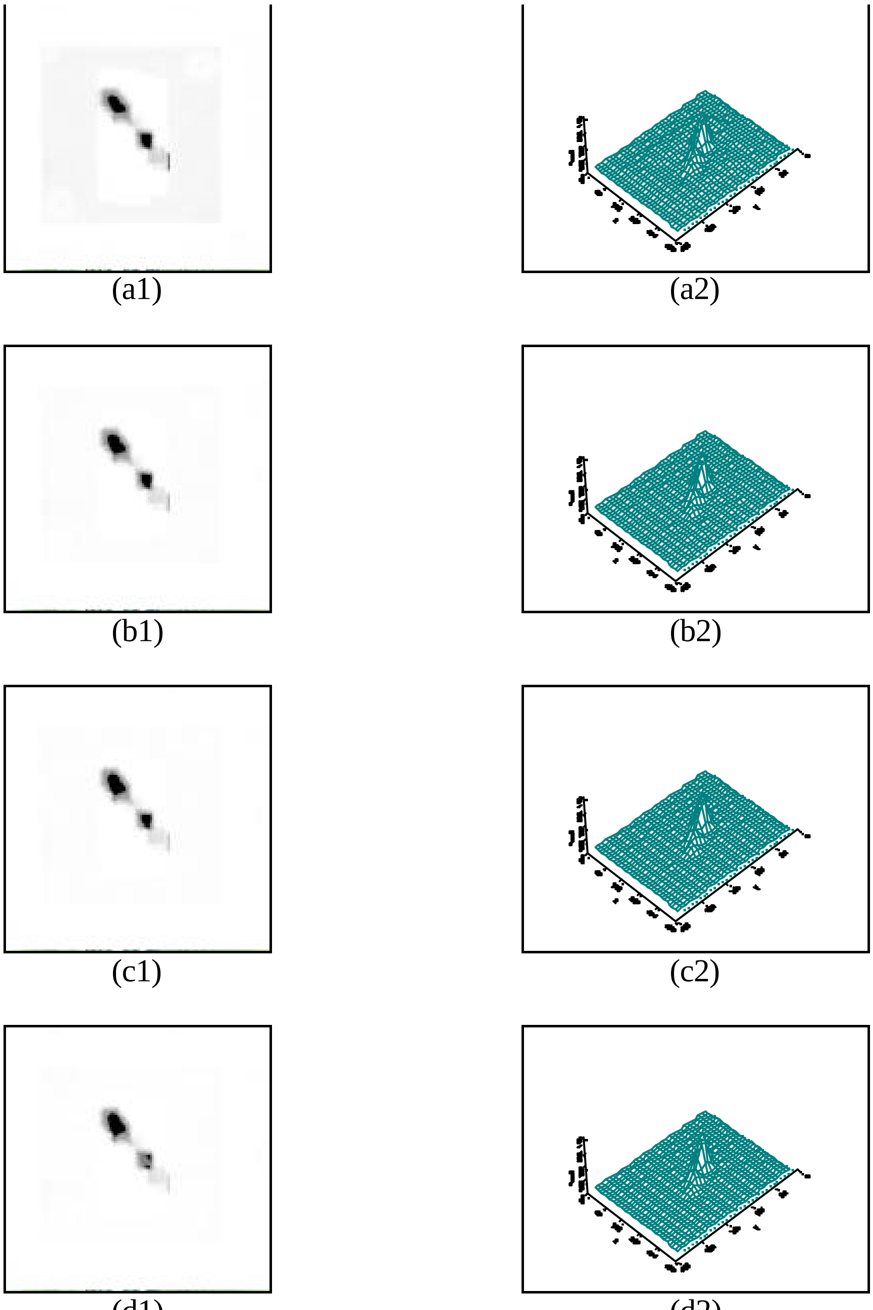

Figure 7. The effect of smoothing on defective color images in Figure 6: (a1)-(d1) the correlation values d_c as an intensity with smoothing filter sizes of nil, 3×3, 5×5 and 7×7, respectively; (a2)-(d2) the respective correlation functions $(1-d_c)$ in 3-D perspective.

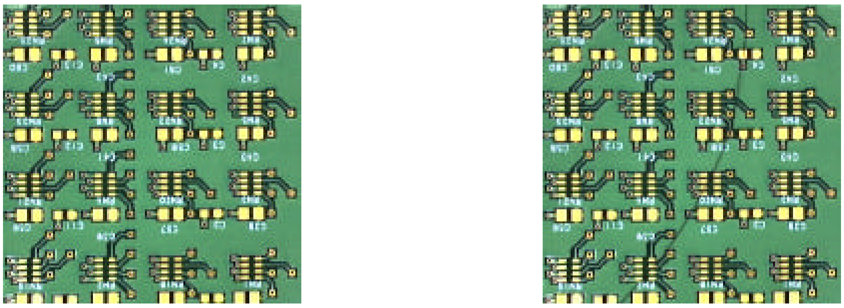

(a) (b)

Figure 8. A test sample of printed circuit board: (a) the reference image; (b) the scene image that contains a subtle scratch.

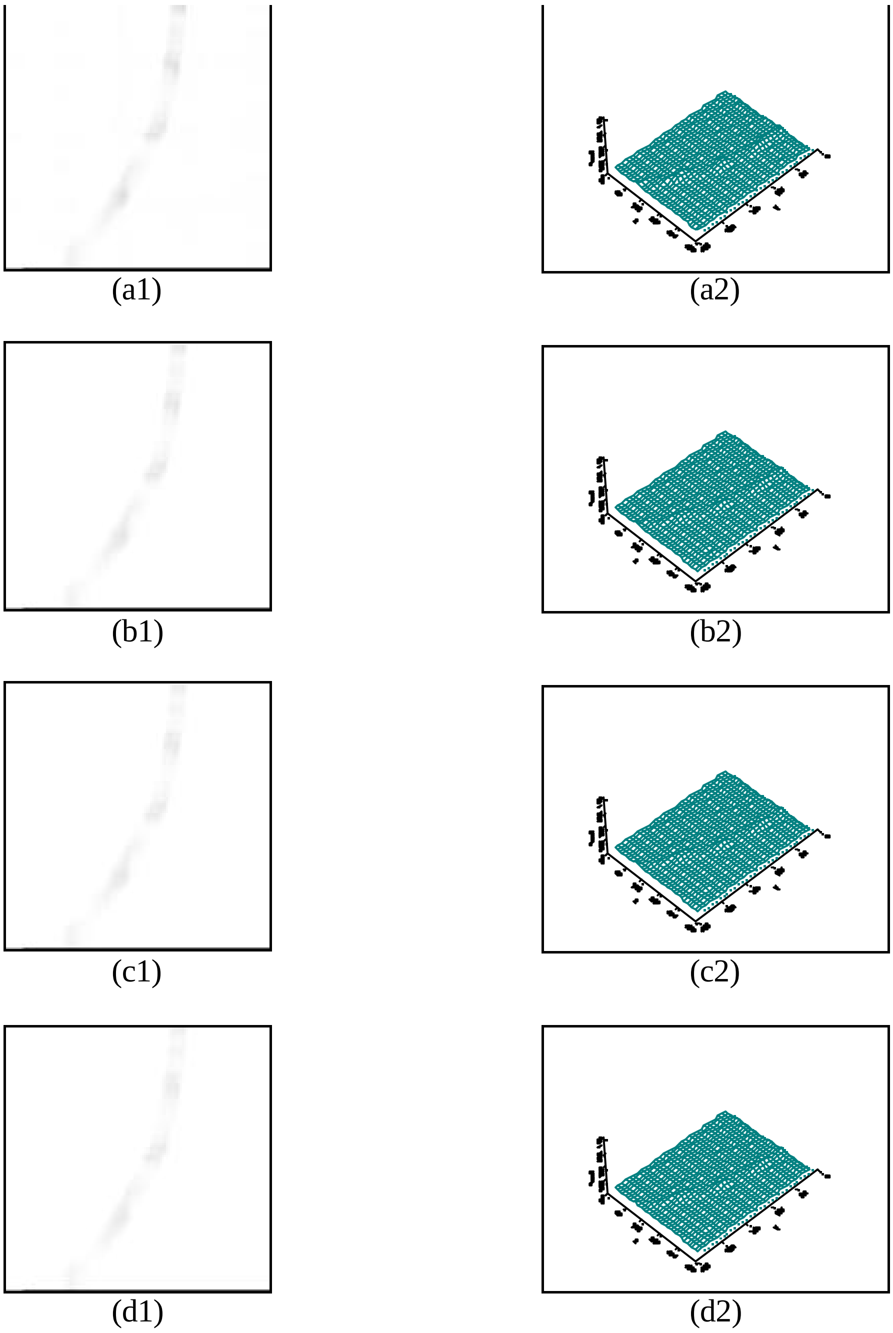

Figure9. The effect of smoothing on color images in Figure 8: (a1)-(d1) the correlation values d_c as an intensity with smoothing filter sizes of nil, 3×3, 5×5 and 7×7, respectively; (a2)-(d2) the respective correlation function $(1-d_c)$ in 3-D perspective.

Table 1. The statistics and signal-to-noise ratios of correlation values d_g and d_c for the IC samples in Figure1.

Statistics	Gray-level image d_g	Color image d_c
Mean of d	0.869	0.989
Standard deviation of d	0.181	0.014
Maximum d	1.000	1.000
Minimum d	0.309	0.958
SN ratio	17.662	39.620

Table 2. The statistics and signal-to-noise ratios of d_g and d_c from the images in Figure1 with varied smoothing filter sizes.

Image	Smoothing filter size	Mean	Standard deviation	Max d	Min d	SN ratio
Gray-level d_g	Nil	0.869	0.181	1.000	0.309	17.662
	3×3	0.922	0.120	1.000	0.361	22.175
	5×5	0.926	0.116	1.000	0.367	22.681
	7×7	0.927	0.115	1.000	0.379	22.735
Color d_c	Nil	0.989	0.014	1.000	0.958	39.620
	3×3	0.997	0.004	1.000	0.987	50.620
	5×5	0.998	0.003	1.000	0.991	53.355
	7×7	0.998	0.002	1.000	0.992	54.870